

Spin-phonon coupling, high-pressure phase transitions, and thermal expansion of multiferroic GaFeO₃: A combined first principles and inelastic neutron scattering study

Mayanak Kumar Gupta,¹ Ranjan Mittal,¹ Mohamed Zbiri,² Ripandeep Singh,¹ Stephane Rols,² Helmut Schober,² and Samrath Lal Chaplot¹

¹*Solid State Physics Division, Bhabha Atomic Research Centre, Mumbai 400085, India*

²*Institut Laue-Langevin, 71 Avenue des Martyrs, CS 20156, 38042 Grenoble Cedex 9, France*

(Received 4 June 2014; revised manuscript received 25 August 2014; published 9 October 2014)

We have carried out an extensive phonon study on multiferroic GaFeO₃ to elucidate its dynamical behavior. Inelastic neutron scattering measurements are performed over a wide temperature range, 150 to 1198 K. First principles lattice dynamical calculations are done for the sake of the analysis and interpretation of the observations. The comparison of the phonon spectra from magnetic and nonmagnetic calculations highlights pronounced differences. The energy range of the vibrational atomistic contributions of the Fe and O ions are found to differ significantly in the two calculation types. Therefore, magnetism induced by the active spin degrees of freedom of Fe cations plays a key role in stabilizing the structure and dynamics of GaFeO₃. Moreover, the computed enthalpy in various phases of GaFeO₃ is used to gain deeper insights into the high-pressure phase stability of this material. Further, the volume dependence of the phonon spectra is used to determine its thermal expansion behavior.

DOI: [10.1103/PhysRevB.90.134304](https://doi.org/10.1103/PhysRevB.90.134304)

PACS number(s): 78.70.Nx, 63.20.-e, 65.40.-b

I. INTRODUCTION

Materials showing more than two ferroic properties (magnetism, electricity, and elasticity) simultaneously come under the umbrella of multiferroics, whose characteristics include the emergence of simultaneous electric and magnetic orderings, therefore offering opportunities for multifunctional device applications. This justifies the intense research going on with this class of materials and the keen interest they are subject to on both the fundamental and practical sides [1–14]. In materials containing transition metals, magnetism is induced by the active spin components in the *d* shell levels. On the other hand, ferroelectricity occurs generally in the absence of *d* electrons. Hence, it is intriguing to observe multiferroicity since this phenomenon involves a simultaneous emergence of both properties. Over the last few decades, various multiferroic materials have been discovered that exhibit magnetoelectric (ME) coupling. However, most of the ME multiferroics possess magnetic and ferroelectric transition temperatures far from the ambient one. For example, in the case of BiMnO₃ [14], the Curie temperature T_C is about 100 K, while the Néel temperature T_N is close to 750 K. This results in a weak ME coupling under the ambient conditions. Practically, the weak coupling materials are not potentially useful. However, there are few mechanisms that allow tuning these properties simultaneously, such as magnetic ferroelectricity induced by frustrated magnetism, the lone pair effect, charge ordering, and local noncentrosymmetry. For instance, charge ordering driven magnetic ferroelectricity is observed in a large number of rare earth oxides [11,12]. Understanding the mechanism of multiferroicity is of considerable importance for the design of new multiferroics at controllable conditions (temperature and pressure). Hence, the electric and magnetic properties attributed to the dynamics of ions and electrons need to be studied and explored.

GaFeO₃ belongs to the class of multiferroic compounds and shows a ME coupling at low temperature. It does not contain lead or bismuth species, making it ecologically and

biologically attractive. At room temperature, the structure [15] is chiral orthorhombic ($Pc2_1n$), while its parental oxides Fe₂O₃ and Ga₂O₃ occur [16] in the rhombohedral and monoclinic phases, respectively. The orthorhombic structure of GaFeO₃ has eight formula units per unit-cell, with two different symmetry inequivalent sites of iron and gallium atoms; Fe1, Fe2, Ga1, and Ga2, respectively. The tetrahedral sites are occupied by Ga1, while Ga2, Fe1, and Fe2 occupy all the octahedral sites (Fig. 1). The electric polarization is found [15] to be along the *b* axis at ambient conditions. Ideally, the magnetic structure of GaFeO₃ is expected to reflect an antiferromagnetic ordering, since the magnetic moments of Fe1 and Fe2 cations are antiparallel. However, due to the observed disorder on the Fe and Ga sites [15], a ferrimagnetic transition is observed below 225 K instead [15,17]. The magnetization axis was found to be along the *c* axis.

In a first principles study, Han *et al.* and Stoeffler [18] suggest that distorted octahedra, GaO₆ and FeO₆, in GaFeO₃ lead to a noncentrosymmetric structure, which might be responsible for the electric polarization. The authors also showed that the site disorder involving the interchange of Fe and Ga2 sites is highly probable and consistent with the presence of the observed Fe disorder [15] with the Ga2 site. They indicate that the minimum of total energy is reached when adopting an antiferromagnetic spin configuration. However, antisite disorder of Fe and Ga atoms between octahedral Ga and Fe sites lead to a finite magnetic moment, and GaFeO₃ behaves like a ferrimagnet. It has been concluded that the significant orbital magnetic moment of Fe ions is attributed to the local distortion of oxygen octahedra and the off centering of the iron atoms.

Interestingly, the unequal distribution of Fe spins in GaFeO₃ is due to the Ga-Fe disorder. This material is known to exhibit piezoelectricity and ferrimagnetism with a Curie temperature T_C of about 225 K. This could be enhanced by a site disorder between Ga and Fe. It has been shown that the T_C could be enhanced [19] to ~350 K by increasing the Fe content to about 40% (Ga_{2-x}Fe_xO₃ ($x = 1.40$)). The magnetic structure and ME

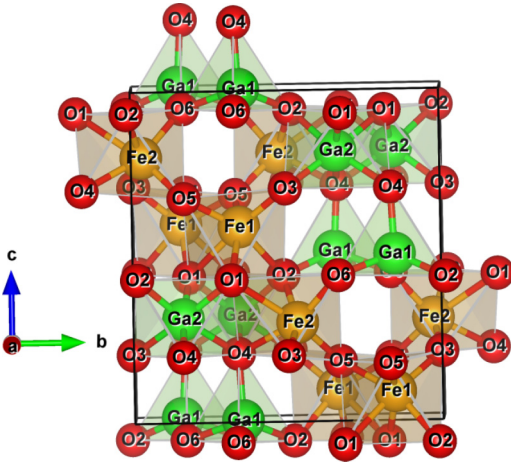


FIG. 1. (Color online) Crystal structure of GaFeO_3 in the $Pc2_1n$ space group. The atoms are labeled following Table I.

properties of $\text{Ga}_{2-x}\text{Fe}_x\text{O}_3$ ($0 < x < 1.1$) were extensively studied by Arima *et al.* [15]. The authors found that the saturated magnetization as well as the ferrimagnetic phase transition temperature increases with an increase in Fe content, while the coercive force decreases. The linear and quadratic ME coefficient measurements show that the electric polarization is largely modulated when a magnetic field is applied parallel to the direction of the spontaneous magnetization. However, it has a negligible effect when the field is applied parallel to the spontaneous polarization axis. Thin films of GaFeO_3 are reported to exhibit [20] ferroelectricity at room temperature, which makes them practically useful at the nanolevel. We note also that the ball milling transforms [21] the structure of GaFeO_3 from orthorhombic to rhombohedral ($R3c$).

First principle studies of zone-center phonon modes and Raman measurements were reported on the isostructural compound AlFeO_3 by Kumar *et al.* [22]. The Raman measurements have been performed in the temperature range 5–315 K. The observed spectra showed that the intensity of the Raman mode at 1230 cm^{-1} vanishes to zero above 250 K. It was concluded that this mode originates from a two magnon Raman process. The authors also reported first principles calculation of the zone-center phonon modes in magnetic ordered and disordered structure. They found a strong interaction between spin and lattice vibrations [22].

X-ray as well as neutron diffraction, dielectric, Raman, and infrared (IR) measurements have been reported on GaFeO_3 [23–28]. No structural phase transition was observed [28] in the temperature range 14–1368 K. A dielectric anomaly [24] has been observed at the magnetic transition temperature. A spin-phonon coupling is reported [26] to take place below 210 K by observing the discontinuity in the peak position of the Raman mode at 374 cm^{-1} . Raman and Mossbauer spectroscopic studies on GaFeO_3 have also been reported [27]. The authors observed a disordered nature of the compound. The peak width of the phonon mode at 700 cm^{-1} shows an anomalous large broadening around the Curie temperature, which is a measure of anharmonicity. The data were interpreted within the context of coupling of phonons and the Fe spins. Further, the stability of GaFeO_3 has

been studied [29] under pressure; up to about 65 GPa. The compound undergoes a phase transition [29] from $Pc2_1n$ to $Pbnm$ phase at about 25 GPa. Increasing further the pressure to 53 GPa, the $Pbnm$ phase also undergoes first order phase transition due to quenching of the Fe magnetic moment. Spin wave measurements have been reported by inelastic neutron scattering [30–32] in similar systems (TmFeO_3 , ErFeO_3 , YFeO_3 , and TbFeO_3). An incommensurate phase was evidenced [32] in TbFeO_3 , upon applying a magnetic field.

The various studies available on GaFeO_3 are based on structural and electronic considerations. A limited amount of work on phonon dynamics has been reported, but it was restricted to the zone-center phonon modes. Presently, we provide a detailed analysis of lattice dynamics and spin phonon coupling in GaFeO_3 , where both the zone-center and zone-boundary modes are covered. A better understanding of the dynamics governing the thermodynamical aspects of this promising multiferroic is necessary for future fundamental and practical developments. In this context, we have measured the phonon density of states over a wide temperature range, 150–1198 K. We have computed the phonon spectrum from first principles density functional theory to quantitatively explore the dynamics. The study is done in the ordered phase by first considering the magnetic interactions and then neglecting them to better explore the possible interplay and effect of the spin degrees of freedom on the lattice dynamics [33,34]. Further, the total energy and enthalpy is estimated in various phases to determine the relative phase stability of GaFeO_3 . The equation of state has been calculated and compared with the available experimental data. Additionally, the volume thermal expansion has also been calculated as to have a better view on the thermodynamical picture of GaFeO_3 .

Our paper is organized as follows: Secs. II and III provide details on the inelastic neutron scattering investigations and computational technicalities, respectively. The results are discussed in four parts in Secs. IV A–IV D: Sec. IV A deals with the temperature dependence of phonon spectra; Sec. IV B highlights the effect of magnetic ordering on the calculated phonon spectra; in Sec. IV C, we treat essentially total energy and free energy calculations for the phase diagram purpose; and the thermal expansion behavior is given in Sec. IV D. Finally, conclusions are drawn in Sec. V.

II. EXPERIMENTAL DETAILS

The inelastic neutron scattering measurements were carried out using the direct-geometry thermal neutron IN4C spectrometer at the Institut Laue Langevin (ILL), France. The spectrometer is based on the time-of-flight technique and is equipped with a large detector bank covering a wide scattering angle range of about 10° to 110° . The polycrystalline sample of GaFeO_3 was prepared using the solid state reaction method [15]. About 10 grams of the polycrystalline sample of GaFeO_3 was used for the measurements. The measurements were performed at several temperatures in the range 150–1198 K. The low temperature measurements were performed using a standard orange cryostat. For the high temperature range, the sample was put into a quartz tube insert and mounted into a furnace. The other end of the quartz tube was kept in open air.

TABLE I. Comparison between the experimental (4 K) and calculated (0 K) structural parameters of GaFeO₃ (orthorhombic phase, space group $Pc2_1n$). The experimental structure (space group $Pc2_1n$) consists [15] of all the atoms at $4a(x, y, z)$. Wyckoff site with site occupancies of 1.0, 1.0, 1.0, 1.0, 1.0, 1.0, 0.82/0.18, 0.65/0.35, 0.23/0.77, and 0.30/0.70 of O1, O2, O3, O4, O5, O6, Ga1(Ga/Fe), Ga2(Ga/Fe), Fe1(Ga/Fe), and Fe2(Ga/Fe) atomic sites, respectively. The *ab initio* calculations were performed adopting an integer site occupancy. FM, FNM, and PNM refer to fully relaxed magnetic, fully relaxed nonmagnetic, and partially relaxed nonmagnetic calculations, respectively.

		Expt.	FM (GGA)	FM (LDA)	PNM (LDA)	FNM (LDA)
	a (Å)	8.7193	8.8516	8.6610	8.6610	8.4791
	b (Å)	9.3684	9.5232	9.2923	9.2923	8.7713
	c (Å)	5.0672	5.1491	5.0355	5.0355	4.9999
O1	x	0.3228	0.3221	0.3233	0.3154	0.3255
	y	0.4262	0.4268	0.4291	0.4405	0.4517
	z	0.9716	0.9825	0.9836	0.9860	0.9802
O2	x	0.4864	0.4868	0.4857	0.4853	0.4789
	y	0.4311	0.4323	0.4330	0.4413	0.4555
	z	0.5142	0.5190	0.5190	0.5331	0.5312
O3	x	0.9979	0.9970	0.9969	0.9877	0.9851
	y	0.2022	0.2022	0.2014	0.2091	0.2216
	z	0.6541	0.6579	0.6564	0.6599	0.6605
O4	x	0.1593	0.1615	0.1621	0.1564	0.1590
	y	0.1974	0.1996	0.2005	0.2049	0.2123
	z	0.1480	0.1570	0.1575	0.1684	0.1662
O5	x	0.1695	0.1683	0.1677	0.1667	0.1651
	y	0.6717	0.6726	0.6742	0.6820	0.7001
	z	0.8437	0.8422	0.8447	0.8245	0.8309
O6	x	0.1736	0.1671	0.1664	0.1658	0.1632
	y	0.9383	0.9391	0.9394	0.9365	0.9509
	z	0.5166	0.5180	0.5217	0.5247	0.5372
Fe1	x	0.1538	0.1539	0.1549	0.1678	0.1709
	y	0.5831	0.5834	0.5836	0.5894	0.6049
	z	0.1886	0.1857	0.1883	0.1691	0.1689
Fe2	x	0.0346	0.0316	0.0308	0.0269	0.0186
	y	0.7998	0.7956	0.7961	0.8000	0.8168
	z	0.6795	0.6721	0.6739	0.6772	0.6785
Ga1	x	0.1500	0.1520	0.1510	0.1503	0.1462
	y	0.0	0.0	0.0000	0.0000	0.0000
	z	0.1781	0.1749	0.1770	0.1789	0.1873
Ga2	x	0.1593	0.1608	0.1607	0.1561	0.1589
	y	0.3073	0.3089	0.3095	0.3139	0.3204
	z	0.8106	0.8167	0.8160	0.8189	0.8181

For these measurements, we have used an incident neutron wavelength of 2.4 Å (14.2 meV), performing in the upscattering mode (neutron energy gain). The momentum transfer Q extends up to 7 Å⁻¹. In the incoherent one-phonon approximation, the measured scattering function $S(Q, E)$, as observed in the neutron experiments, is related [35] to the phonon density of states $g^{(n)}(E)$ as follows:

$$g^{(n)}(E) = A \left\langle \frac{e^{2W_k(Q)}}{Q^2} \frac{E}{n(E, T) + \frac{1}{2} \pm \frac{1}{2}} S(Q, E) \right\rangle, \quad (1)$$

$$g^n(E) = B \sum_k \left\{ \frac{4\pi b_k^2}{m_k} \right\} g^k(E), \quad (2)$$

where the + or - signs correspond to energy loss or gain of the neutrons, respectively, and where $n(E, T) = [\exp(E/k_B T) - 1]^{-1}$. A and B are normalization constants and b_k , m_k , and $g^k(E)$ are, respectively, the neutron scattering length, mass, and partial density of states of the k th atom in the unit cell. The quantity between $\langle \rangle$ represents a suitable

average over all Q values at a given energy. $2W(Q)$ is the Debye-Waller factor. The weighting factors $\frac{4\pi b_k^2}{m_k}$ for various atoms in the units of barns per atomic mass unit are Ga: 0.098, Fe: 0.208, and O: 0.265. The values of the neutron scattering lengths are taken from Ref. [36].

III. COMPUTATIONAL DETAILS

Relaxed geometries and total energies were obtained using the projector-augmented wave (PAW) formalism [37,38] of the Kohn-Sham density functional theory [39,40], within both the local density approximation (LDA) and the generalized gradient approximation (GGA), implemented in the Vienna *Ab initio* Simulation Package (VASP) [41]. The GGA was formulated by the Perdew-Burke-Ernzerhof (PBE) density functional [42]. The LDA was based on the Ceperley-Alder parametrization by Perdew and Zunger [43]. The valence electronic configurations of Ga, Fe, and O as used in calculations for pseudopotential generation are $s^2 p^1$, $d^7 s^1$, and

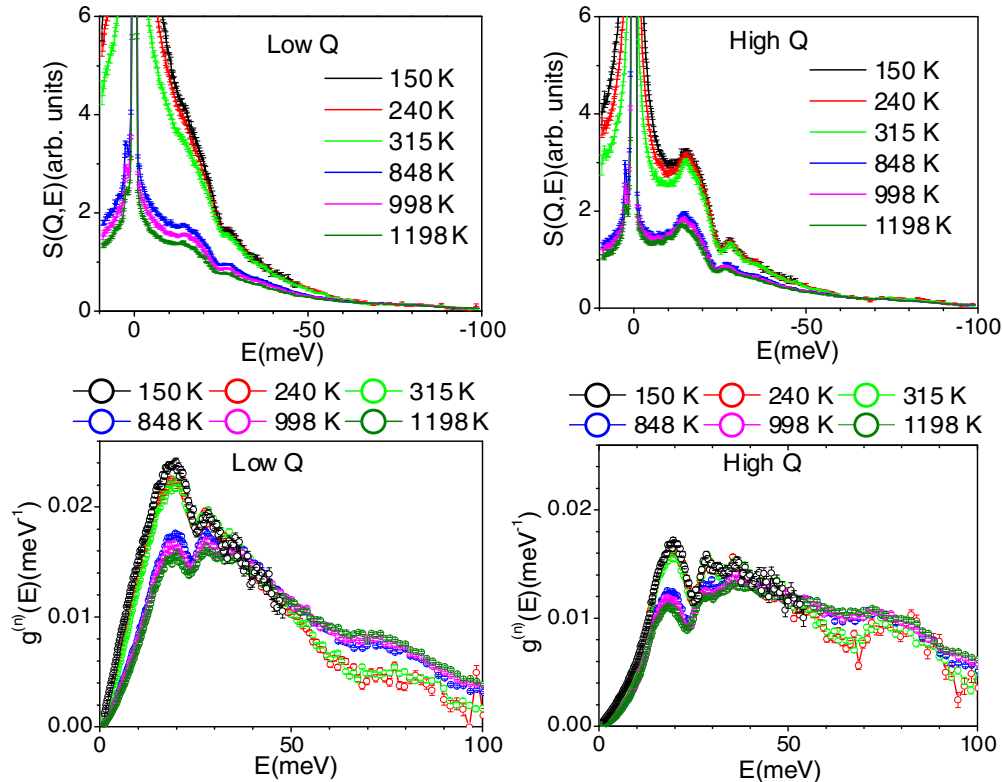


FIG. 2. (Color online) Temperature dependent inelastic neutron spectra of GaFeO₃. Top panel: the low Q and high Q Bose factor corrected $S(Q, E)$, where both the energy loss (0–10 meV) and the energy gain (–100–0 meV) sides are shown. Bottom panel: the low Q and high Q , unity-normalized, phonon density of states, $g^{(n)}(E)$, inferred from the neutron energy gain mode $S(Q, E)$ data within the incoherent approximation.

s^2p^4 , respectively. Both non-spin-polarized and spin-polarized calculations were performed. The magnetic calculations have been carried out for the A-type antiferromagnetic ordering in the $Pc2_1n$ phase. Moreover, since GaFeO₃ is known to be a Mott insulator, the onsite Hubbard correction is applied using the Dudarev approach [44] using $U_{\text{eff}} = 4$ eV [45–49].

Both full (lattice constants and atomic positions) and partial (only atomic positions) geometry relaxations were carried out. Hereafter, the labeling “FM” and “FNM” refer to fully relaxed magnetic and fully relaxed nonmagnetic calculations. Further, “PNM” refers to the partially relaxed nonmagnetic calculation, where we used the structure obtained from FM and relaxed only the atomic positions without magnetic ordering. The structural details relevant to the present calculations are summarized in Table I. Further, we performed fully relaxed magnetic calculations (labeled as FM_Ga_SC) including the semicore electrons of the Ga atoms having the electronic configuration $d^{10}s^2p^1$. The equation of states as well as the free energy of GaFeO₃ have also been evaluated in the fully relaxed magnetic calculations (labeled as FM_GaFe_SC) by considering $d^{10}s^2p^1$ and $p^6d^7s^1$ electronic configuration for Ga and Fe atoms, respectively.

All results were well converged with respect to k-mesh and energy cutoff for the plane wave expansion. The break conditions for the self-consistent field (SCF) and for the ionic relaxation loops were set to 10^{-8} eV and 10^{-5} eV \AA^{-1} , respectively. The latter break condition means that the obtained Hellmann-Feynman forces are less than 10^{-5} eV \AA^{-1} .

A $4 \times 4 \times 4$ k-point mesh for the Brillouin zone integration was found to be suitable for the required convergence. The energy cutoffs were set to 620, 720, and 740 eV for the calculations carried out with soft pseudopotentials, then including only the Ga semicore electrons, and also with semicore electrons of both Ga and Fe, respectively. Total energies were calculated for 60 generated structures resulting from individual displacements of the symmetry inequivalent atoms in the orthorhombic ($Pc2_1n$) phase, along the six inequivalent Cartesian directions ($\pm x$, $\pm y$, and $\pm z$). Phonons are extracted from subsequent calculations using the direct method as implemented in the Phonon software [50]. The free energy calculations of GaFeO₃ are also done in the $Pbnm$ and $R3c$ phases.

IV. RESULTS AND DISCUSSION

A. Temperature dependence of phonon spectra

The phonon spectra of GaFeO₃ (Fig. 2) were measured up to 1198 K, across the magnetic transition (~ 225 K). The magnetic signal is expected to be more pronounced at low Q , and to vanish at high Q , following the magnetic form factor. Therefore, two Q domains were considered; i.e., high Q (4 to 7 \AA^{-1}) and low Q (1 to 4 \AA^{-1}).

The temperature dependence of the Bose factor corrected $S(Q, E)$ plots of GaFeO₃ are shown in Fig. 2. At low temperatures (up to 315 K), the low Q data show a larger elastic line as compared to the high Q spectra. Presently, given the lack of detailed magnetic measurements, we speculate that this

quasielastic scattering may originate from spin fluctuations that disappear at high temperatures. In the high temperature range, only phonons contribute significantly to the spectra, and therefore the width of the elastic line is similar in both the Q ranges.

The phonon spectra inferred from the $S(Q, E)$ data, within the incoherent approximation, are also shown in Fig. 2. The phonon spectra consist of several peaks located around 20, 30, 55, and 80 meV. We find that both the high Q as well as the low Q data show large variation in the intensity as a function of temperature. At low energy (below 40 meV), the low Q data are more intense in comparison to the high Q data. Further, for the low Q part, at 150 K below the magnetic transition temperature (~ 225 K), there is a large intensity of the low energy inelastic spectra (~ 20 meV) as compared to the data collected at higher temperatures. This is expected to be due to a strong magnetic signal. At 848 K, it is found that in both the low Q as well as the high Q data, there is a considerable decrease of the intensity of the low energy peaks around 20 meV. Although GaFeO_3 undergoes a paramagnetic to ferrimagnetic transition on cooling [15] around 225 K, a paramagnetic scattering persists in the low energy range around 20 meV, at 240 and 315 K. The intensity in the higher energy range, above 55 meV, of the high Q data does not show significant temperature dependence, confirming a pure phonon contribution in this spectral regime. Above 848 K, there is a loss of intensity, due to paramagnetic scattering, and only phonons contribute in this range.

GaFeO_3 does not show any structural phase transition at high temperature. However, polyhedral (GaO_4 , GaO_6 , FeO_6) distortions are found to increase upon heating up to 1198 K [28]. This might be an additional reason for the broadening of the phonon spectra above 60 meV at high temperatures, besides the increased thermal amplitudes.

B. Magnetic ordering and calculated phonon spectra

The microscopic origin of the polarization in multiferroic materials is attributed to the hybridization of the electronic orbitals producing a polar charge distribution and ionic displacements from the related centrosymmetric positions. Hence, it is important to study the lattice dynamics in order to understand the ME properties of multiferroics. Detailed electronic structure calculations of GaFeO_3 are reported in the literature [18]. However, phonon studies over the whole Brillouin zone are missing. Calculations of (electronic) structure and dynamics would help to gain newer and deeper insights into the various physical properties and possible phase transitions of these kinds of materials.

The calculated Fe magnetic moment in the equilibrium structure in the $Pc2_1n$ phase at Fe1 and Fe2 sites are both $4.1 \mu_B$, which is in agreement with the reported experimental values [15] of 3.9 and $4.5 \mu_B$. Neglecting the spin degrees of freedom in the calculations leads to a collapse of the b lattice parameter, with a value decreasing from 9.29 to 8.77 \AA . However, by considering Fe magnetism, the calculated value of the b lattice parameter is brought to agreement with the observation (Table I).

Figure 3 compares the experimental and calculated phonon spectra. The FNM calculation results in a shift of all the

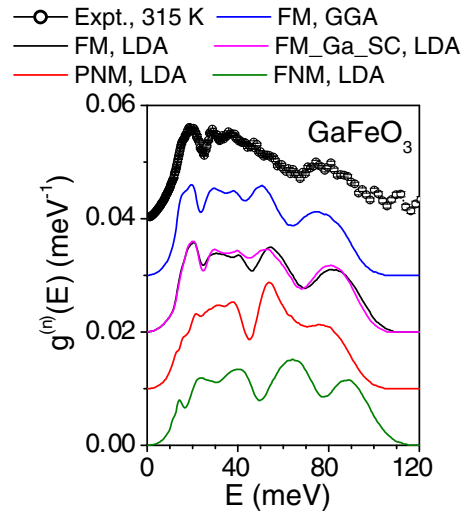


FIG. 3. (Color online) The calculated and experimental neutron inelastic scattering spectra of GaFeO_3 . The experimental data consist of the high Q data collected at 315 K. The calculated spectra have been convoluted with a Gaussian of full width at half-maximum (FWHM) of 15% of the energy transfer in order to describe the effect of energy resolution in the experiment. All the spectra are normalized to unity in the entire spectral range. FM, FNM, and PNM refer to fully relaxed magnetic, fully relaxed nonmagnetic, and partially relaxed nonmagnetic calculations, respectively. FM_Ga_SC refers to the fully relaxed magnetic calculations including the semicore electrons of Ga atoms. For better visibility, the experimental and calculated phonon spectra are shifted vertically with respect to each other.

modes to higher energies. This is due to the fact that the b axis is underestimated in FNM calculations, leading to an overestimation of the phonon energies. Interestingly, the model calculations FM and PNM provide a very good agreement with the experimental spectra. We notice, however, some differences in the low energy part of the phonon spectra. The difference comes in fact from the value of the Fe magnetic moment in the two numerical models. The main effect of the Fe spin degrees of freedom is to soften the calculated phonon energies around 30 meV, thus bringing them closer to the experimental values. This demonstrates the role of magnetic interactions in GaFeO_3 in a similar way to other recent phonon studies in other systems [33,34].

The FM-based calculated phonon spectra (Fig. 3) lead to peaks centered around 20, 30, 55, and 80 meV. The experimental spectra show peaks at 20 and 30 meV and clear humps at 55 and 80 meV. GaFeO_3 is known to have a Ga-Fe disorder, from diffraction measurements [15]. However, our phonon calculations were done in the ordered phase (Table I). The structural disorder could lead to a large variation of the Ga/Fe-O bonds and would then result in a broadening of the peaks, as experimentally observed.

The difference in the phonon spectra (Fig. 3) from the various calculations can be understood from the estimated atomistic contributions in terms of the partial density of states from LDA calculations (Fig. 4). The difference is primarily due to the nature of the chemical bonding, in the magnetic and nonmagnetic configurations, as well as the related volume effect. We find that vibrations of Fe and Ga atoms extend

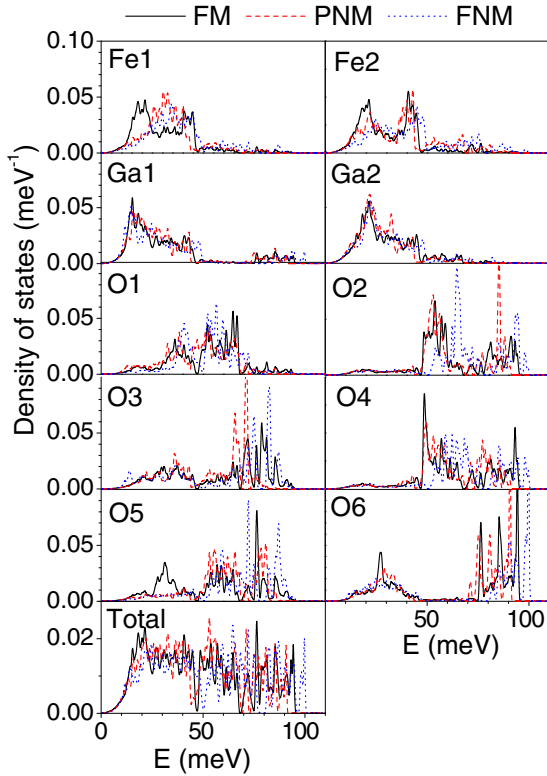


FIG. 4. (Color online) The calculated partial phonon density of states of various atoms in GaFeO_3 within the LDA. The atoms are labeled following Table I. FM, FNM, and PNM refer to fully relaxed magnetic, fully relaxed nonmagnetic, and partially relaxed nonmagnetic calculations, respectively.

up to 45 meV, while the dynamics of the oxygen atoms spread over the entire spectral range, up to 100 meV. The vibrational aspects due to the two Ga symmetry inequivalent atomic sites remain nearly invariant in all three calculation types, while the Fe vibrations show a considerable change. The intensity of vibrational density of states of the Fe2 atoms is enhanced around 20 meV. The vibrations of Fe1 as calculated around 30 meV in the nonmagnetic calculations are found to soften magnetically and exhibit a peak around 20 meV. FNM calculations predict the oxygen vibrations to extend up to about 100 meV. The overestimation in the range of vibrations is primarily due to the noninclusion of the Fe magnetic moment which results in a contraction of the unit cell. The FM and PNM model calculations show that the vibrations of all the oxygen atoms soften in the energy range 60–100 meV. A further interesting finding consists of the vibrations of the O5 atoms as extracted from the FM calculation type. The O5 atoms are connected only to the Fe1 and Fe2 atoms (Fig. 1). The O5 vibrations (Fig. 4) around 60 meV are related to the Fe magnetism. This dynamic is found to shift to lower energies at about 30 meV in the FM calculations.

Given the known effect of the density functional approximation (LDA or GGA) on the volume description (LDA tends to underestimate the volume value, and GGA shows the opposite trend), we compare the FM calculated phonon spectra from LDA and GGA approaches. The unit cell volumes from LDA and GGA calculations are estimated to be 405.3 and 434 \AA^3 ,

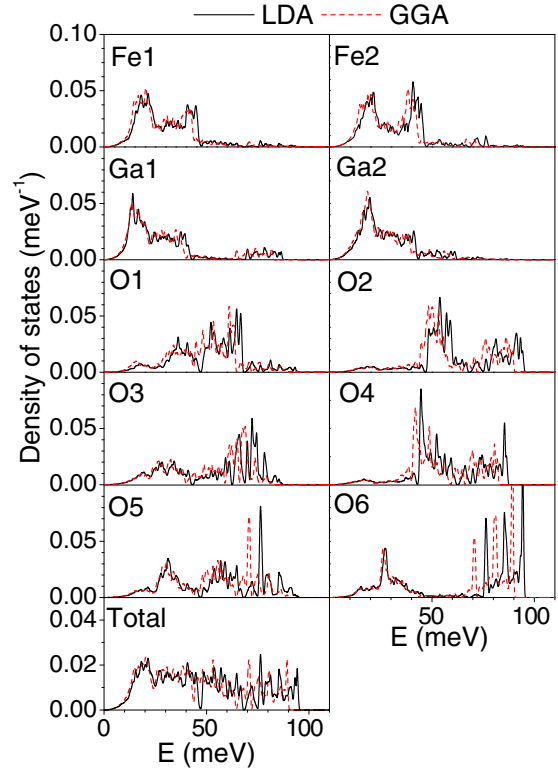


FIG. 5. (Color online) The calculated partial phonon density of states of various atoms in GaFeO_3 within the LDA and the GGA in the FM structure in $Pc2_1n$ space group. The atoms are labeled following Table I.

respectively. The experimental value is 413.9 \AA^3 [15]. The low energy part of the phonon spectra, which is sensitive to Fe magnetism, is nearly the same in both LDA and GGA (Figs. 3 and 5). Above 50 meV, some variations are noticed, however. The GGA calculated phonons above 50 meV are found to be slightly at lower energies as compared to LDA calculated phonons. Both the exchange-correlation methods lead to an overall good matching with the observations.

Under the orthorhombic ($Pc2_1n$) symmetry, GaFeO_3 possesses 120 zone-center modes corresponding to the irreducible representations: $\Gamma = 30A_1 + 30A_2 + 30B_1 + 30B_2$. Figure 6 compares the determined zone-center phonon modes from the various calculation types. The LDA and GGA approximations lead basically to the same phonon energies. Several modes are found to significantly differ when comparing the magnetic and nonmagnetic cases. This confirms a spin-phonon coupling behavior. The change in energies of the modes below 25 meV is mainly due to the magnetic interactions, while the high energy phonons are influenced by the volume effect.

Further, fully relaxed magnetic calculations (FM_Ga_SC) including the semicore electrons of the Ga atoms ($d^{10}s^2p^1$) are performed. The detailed comparison of the FM and FM_Ga_SC calculated phonon spectra (Figs. 3 and 7) shows that the low energy phonons below 40 meV are not affected by the inclusion of the semicore d shell electrons of the Ga atoms. The only noticeable difference is detected in the high energy modes which soften by about 1 meV. Both the calculations are in good agreement with the experimental data. The calculated

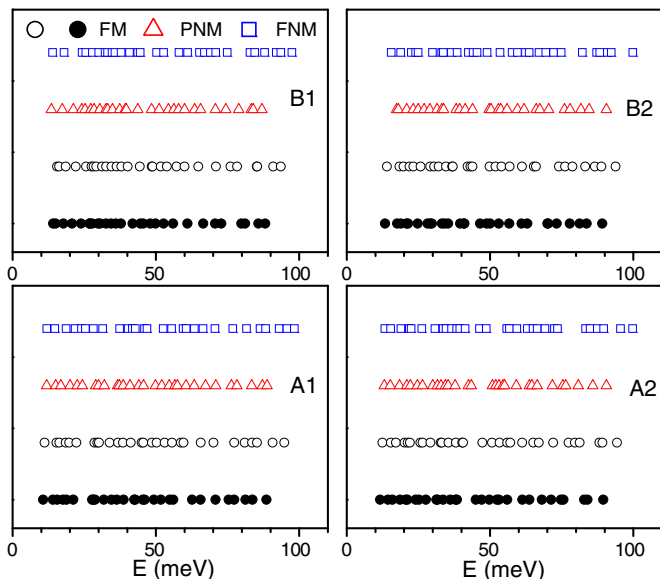


FIG. 6. (Color online) The calculated zone-center phonon modes of GaFeO₃ (orthorhombic phase, space group $Pc2_1n$). FM, FNM, and PNM refer to fully relaxed magnetic, fully relaxed nonmagnetic, and partially relaxed nonmagnetic calculations, respectively. Open and closed symbols correspond to calculations performed within the LDA and GGA, respectively. A1, A2, B1, and B2 correspond to the group theoretical representations of the system symmetry.

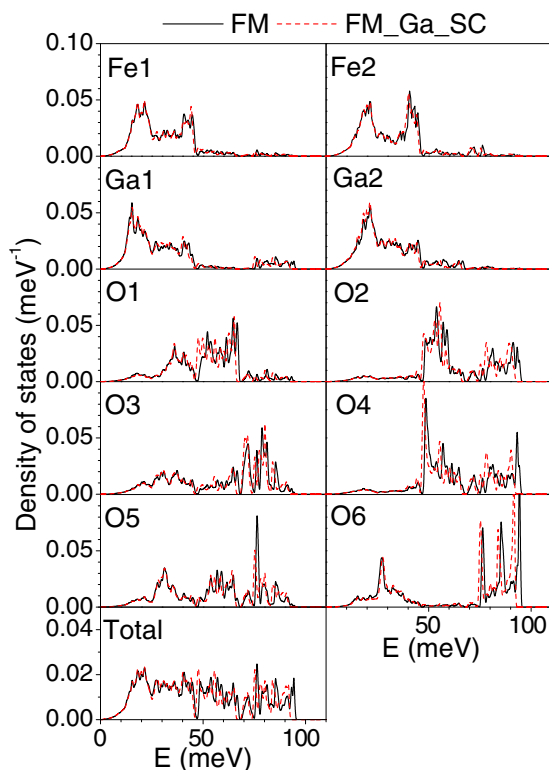


FIG. 7. (Color online) The calculated partial phonon density of states of various atoms in GaFeO₃ within the LDA in $Pc2_1n$ space group. FM_Ga_SC and FM refer to the fully relaxed magnetic calculations with and without the semicore electrons of the Ga atoms, respectively. The atoms are labeled following Table I.

partial densities of states (Fig. 7) indicated that the changes in the high energy range are associated with the change in the partial contribution of O atoms.

C. High-pressure phase stability of GaFeO₃

The high-pressure measurements [29], up to 70 GPa (increasing and decreasing cycles), revealed a very rich phase diagram of GaFeO₃. Arielly *et al.* [29] reported the emergence of a new orthorhombic phase (space group $Pbnm$) above 25 GPa upon increasing pressure. The transition was found to fully establish at 45 GPa. In this phase, all the Ga atoms have eight coordinations. However, in the $Pc2_1n$ phase, two different Ga sites are distinguishable; one with a sixfold symmetry and the other possessing a fourfold coordination. Further increasing the pressure to about 53 GPa results in another first order transition with a significant drop of the volume. However, the system remains in the same orthorhombic space group ($Pbnm$). At this pressure value (53 GPa), the magnetic interactions weaken due to the broadening of the iron d bands. Mossbauer measurement reveals that the Néel temperature is close to 5 K at about 77 GPa. Further decreasing the pressure to the ambient value, the hexagonal $R3c$ phase was found to be the stable one, which is different from the originally starting orthorhombic $Pc2_1n$ phase, at ambient conditions.

In the literature [29], only the lattice parameters of GaFeO₃ are available in the $Pbnm$ and $R3c$ phases. The related atomic coordinates are missing. We have therefore started from the atomic coordinates of LuFeO₃ and LiNbO₃, as provided in Refs. [51,52], respectively. Mossbauer spectroscopy reveals the existence of magnetic ordering in GaFeO₃ [29] even at high pressures. The crystal structure of GaFeO₃ in $Pbnm$ and $R3c$ phases has been calculated by relaxing the atomic coordinates as well as lattice parameters. The total energy has been calculated in both the phases in various antiferromagnetic configurations represented by the A, C, and G ordering types. Computationally, we found that the $Pbnm$ phase is the most stable when adopting the G-type antiferromagnetic ordering, while the $R3c$ phase stabilizes with the A-type antiferromagnetism. The calculated structural details under the $Pbnm$ and $R3c$ phases at 25 GPa and ambient pressure, respectively, are given in Table II. Therein, the available experimental lattice parameters are also shown.

Presently, the high-pressure equation of state, total energy (Φ), and enthalpy ($H = \Phi + PV$) of various phases of GaFeO₃ were estimated for the FM configuration. The GGA calculated enthalpy showed that the high-pressure $Pbnm$ phase is more stable than the $Pc2_1n$ phase at ambient pressure. Figure 8(a) presents the enthalpy difference from LDA calculations for the $Pc2_1n$ and $R3c$ phases with respect to the $Pbnm$ phase. Above 23 GPa, the $Pbnm$ phase is found to be stable when compared to $Pc2_1n$. The application of pressure leads to a change in the correlation between the electronic motions and affects the magnetic interaction. A quenching of the Fe magnetic moment in the $Pbnm$ phase is found at 47 GPa, which triggers a sudden drop of the volume and increases the total energy [Fig. 8(b)]. This is in agreement with the high-pressure data [29], which show a similar behavior around 53 GPa. The values of the magnetic moments on the Fe atoms remain at about $4.1 \mu_B$

TABLE II. The calculated structural parameter of GaFeO₃ in the orthorhombic (*Pbnm*) and hexagonal (*R3c*) phases within LDA in the FM structure. In the orthorhombic phase, the O1, O2, Fe, and Ga atoms are located at $4c (x, 1/4, z)$, $8d (x, y, z)$, $4b(1/2, 0, 0)$, and $4c (x, 1/4, z)$, respectively, while in the hexagonal phase, O, Fe, and Fe occupy the positions $36f (x, y, z)$, $12c (0, 0, z)$, and $12c (0, 0, z)$, respectively. The experimental lattice parameters are from Ref. [29].

Orthorhombic <i>Pbnm</i> phase			
	Expt. (25.7 GPa)	Calc. (25 GPa)	
	<i>a</i>	4.948(4)	4.793
	<i>b</i>	5.165(20)	4.965
	<i>c</i>	7.0000(8)	7.241
O1	<i>x</i>		0.413
	<i>y</i>		0.250
	<i>z</i>		0.142
O2	<i>x</i>		0.323
	<i>y</i>		0.076
	<i>z</i>		0.672
Fe	<i>x</i>		0.500
	<i>y</i>		0.000
	<i>z</i>		0.000
Ga	<i>x</i>		0.059
	<i>y</i>		0.250
	<i>z</i>		0.987
Hexagonal <i>R3c</i> phase			
	Expt. (0.2 GPa)	Calc. (0 GPa)	
	<i>a</i>	5.036(2)	4.981
	<i>b</i>	5.036(2)	4.981
	<i>c</i>	13.585(7)	13.425
O	<i>x</i>		0.969
	<i>y</i>		0.333
	<i>z</i>		0.080
Fe	<i>x</i>		0.000
	<i>y</i>		0.000
	<i>z</i>		0.018
Ga	<i>x</i>		0.000
	<i>y</i>		0.000
	<i>z</i>		0.309

from ambient pressure to below 47 GPa and then decrease to $1.0 \mu_B$ at this transition.

The calculated phase diagram is qualitatively in good agreement with the observation. It should be mentioned that it is difficult to identify experimentally the high-pressure equilibrium phases, due to the large hysteresis. Figure 9 shows the comparison between the LDA calculated and experimental relative change of the unit cell volume in various phases of GaFeO₃ as a function of pressure. A very good agreement is noticed between our calculations and the measurements [29] in the *Pc2_{1n}* and *R3c* structures; however, the volume in the *Pbnm* phase is underestimated. Table III gathers the LDA and GGA calculated elastic constants. The estimated bulk modulus values from LDA and GGA calculations in the *Pc2_{1n}* phase are 207 and 178 GPa, respectively. The LDA determined value is found to be in a better agreement with the experimental bulk modulus value (226 GPa) [29]. As expected, the GGA underestimates the elastic constants by about 15% with respect to LDA, given that GGA tends to overestimate the calculated

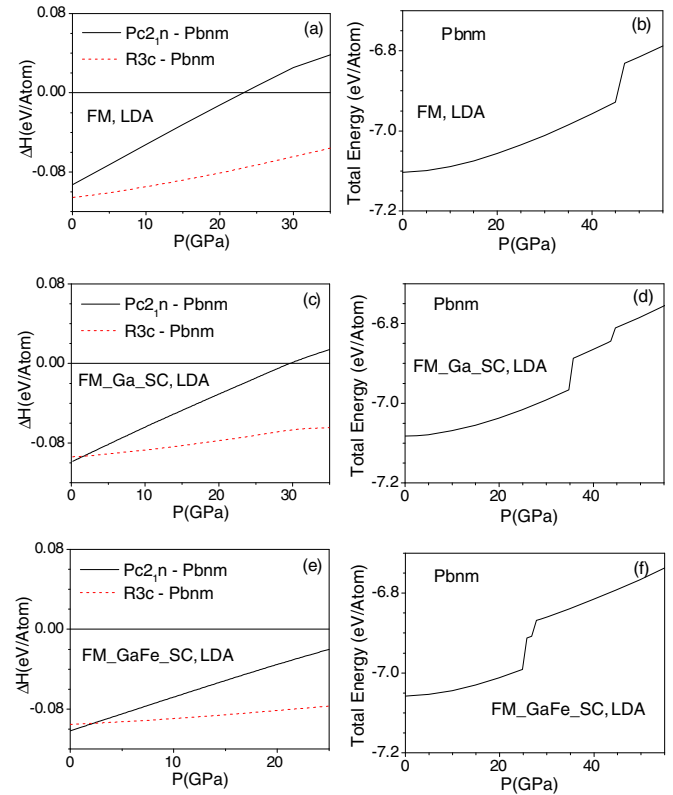


FIG. 8. (Color online) (a), (c), and (e) The calculated enthalpy ($H = \Phi + PV$) difference in the *Pc2_{1n}* and *R3c* phases with respect to the *Pbnm* phase of GaFeO₃ as a function of pressure within the LDA. (b), (d), and (f) The calculated total energy (Φ) in the *Pbnm* phase of GaFeO₃ as a function of pressure within the LDA. The explanation of the labeling FM, FM_Ga_SC, FM_GaFe_SC is described in Sec. III.

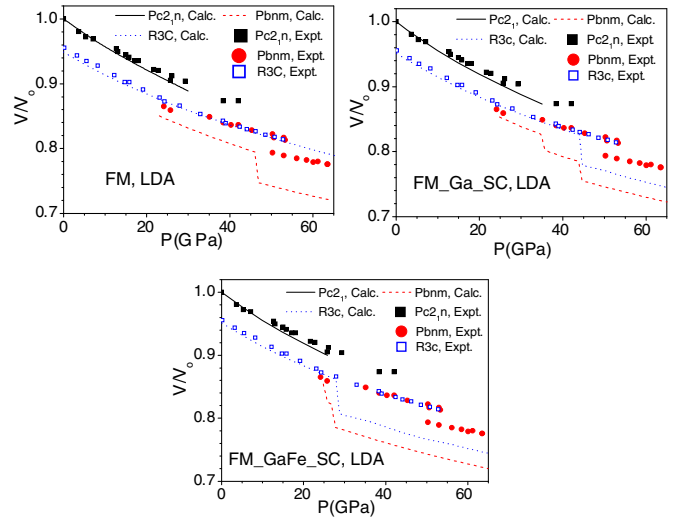


FIG. 9. (Color online) The LDA calculated equation of state of various phases of GaFeO₃ and a comparison with available experimental data [29]. V refers to the volume per formula unit at pressure P . V_0 refers to the volume per formula unit of *Pc2_{1n}* phase at ambient pressure. The explanation of the labeling FM, FM_Ga_SC, and FM_GaFe_SC is described in Sec. III.

TABLE III. The calculated elastic constants (in GPa units) of GaFeO₃ in the orthorhombic phase (space group *Pc2₁n*) in the FM structure at ambient pressure.

Elastic constant	GGA	LDA
C_{11}	291.8	344.6
C_{12}	137.2	163.3
C_{13}	119.8	148.4
C_{22}	257.5	300.0
C_{23}	127.0	159.0
C_{33}	250.3	284.6
C_{44}	62.5	72.7
C_{66}	83.7	95.1

unit cell volume. This results in lowering the calculated bulk modulus values.

Further, the total energy (Φ) and enthalpy ($H = \Phi + PV$) of various phases of GaFeO₃ are estimated from LDA for the fully relaxed magnetic (FM_Ga_SC) configuration including the semicore electrons of the Ga atoms. Here again we found that computationally the *Pbnm* and *R3c* phases are most stable when adopting the G-type antiferromagnetic ordering and A-type antiferromagnetism, respectively. The FM_Ga_SC calculated enthalpy difference in the various phases shows that the *Pbnm* phase is stable above 30 GPa [Fig. 8(c)] when compared to *Pc2₁n*. The pressure increase leads to a quenching of the Fe magnetic moment in the *Pbnm* phase at 36 GPa, resulting in an increase of the total energy [Fig. 8(d)] and a sudden drop of the volume. We also find that the Fe magnetic moment is quenched in the *R3c* phase when the pressure is raised to 45 GPa. The FM_Ga_SC calculated relative change of the unit cell volume as a function of pressure (Fig. 9) in various phases is found to be in qualitative agreement with the experimental data [29].

The environment of the Fe in GaFeO₃ is strongly asymmetric; therefore, polarization of the low-lying semicore states could influence the total energy. In this context, we have also calculated total energy (Φ) and enthalpy ($H = \Phi + PV$) within the LDA framework for the fully relaxed magnetic configuration (FM_GaFe_SC) including the semicore electrons of both the Ga and Fe atoms. As in the above two types of calculations, the G-type and A-type antiferromagnetic ordering is found to be stable for *Pbnm* and *R3c* phases, respectively. The comparison of the enthalpy of the *Pc2₁n* and *Pbnm* phases shows [Fig. 8(e)] that the former phase is stable up to 26 GPa. Further increase in pressure leads to stability of GaFeO₃ in the *Pbnm* phase. This is due to the quenching of the Fe magnetic moment, which leads to an increase of the total energy and a sudden drop of the volume. In the *R3c* phase, the Fe magnetic moment is also found to quench at 28 GPa. A comparison of the experimental [29] and calculated equation of state from FM_GaFe_SC calculations is shown in Fig. 9.

The equation of state is found (Fig. 9) to be qualitatively different as obtained from calculations performed in FM, FM_Ga_SC, and FM_GaFe_SC configurations. We find that a comparison of enthalpy in the *Pc2₁n* and *Pbnm* phases in the FM and FM_Ga_SC calculations reveals a stability of GaFeO₃ in the *Pbnm* phase above 36 and 26 GPa, respectively,

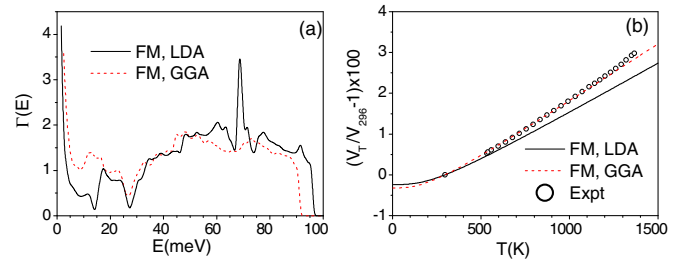


FIG. 10. (Color online) (a) The calculated Grüneisen parameter $\Gamma(E)$ as a function of energy. (b) The calculated and experimental [28] thermal expansion in the orthorhombic phase (space group *Pc2₁n*). FM refers to the fully relaxed magnetic calculations.

while no such phase transition is found in the FM_GaFe_SC calculations. As shown in Fig. 9, quenching of the magnetic moment at high pressure in the *Pbnm* structure induces a number of phase transitions in the different calculations. However, in the *R3c* phase no quenching of the Fe magnetic moment was found in FM calculations. We notice that the Fe moment was found to quench (Fig. 9) in both FM_Ga_SC and FM_GaFe_SC calculations, leading to a phase transition.

The FM calculated enthalpy value under the *Pc2₁n* phase is -7.196 eV/atom, while in the *R3c* phase this is estimated to be -7.209 eV/atom, indicating that the *R3c* phase is more stable as compared to *Pc2₁n*. The calculated energy difference between the two phases is rather small (~ 13 meV/atom). On the other hand, the FM_Ga_SC and FM_GaFe_SC LDA calculated enthalpy values indicate that, at ambient pressure, the *Pc2₁n* phase is energetically favorable by ~ 4 and ~ 6 meV/atom in comparison to the *R3c* phase. However, the *Pc2₁n* phase is found to be stable only below 2 GPa. As discussed and highlighted above, the inclusion of the semicore electrons in the atomistic pseudopotentials has only a minor influence on the obtained dynamical properties, while these seem to induce some qualitative changes in the equation of state.

D. Thermal expansion behavior

The thermal expansion behavior of any material is of considerable importance since it plays a key role for potential applications. The calculation of the thermal expansion of GaFeO₃ is carried out within the quasiharmonic approximation (QHA). In QHA, each phonon mode contributes to the volume thermal expansion coefficient [53,54], given by: $\alpha_V = \frac{1}{BV} \sum_i \Gamma_i C_{Vi}(T)$, where $\Gamma_i (= -\partial \ln E_i / \partial \ln V)$ and C_{Vi} are the mode Grüneisen parameter and the specific heat of the *i*th vibrational state of the crystal, respectively. The volume dependence of phonon modes is calculated in the entire Brillouin zone. The pressure dependence of the phonon spectra in the entire Brillouin zone was extracted from LDA and GGA FM calculations at two pressure points: ambient and 0.5 GPa. Figure 10(a) shows the calculated Grüneisen parameter values, $\Gamma(E)$. They show considerable variation as a function of the energy and are found to lie within 0.2–4.0. The thermal expansion behavior has been calculated up to 1500 K. Neutron diffraction measurements on GaFeO₃ reported the

absence of any high temperature structural phase transition (up to 1368 K) [28]. The comparison between the experimental and calculated thermal expansion character is presented in Fig. 10(b). The GGA leads to a better agreement with the experimental data, while the LDA was found to underestimate the thermal expansion behavior.

V. CONCLUSIONS

We have reported the calculated and measured phonon spectra of the multiferroic material GaFeO₃. The measurements were performed over a wide temperature range (150–1198 K), covering all the relevant characteristic transition temperatures. Across the magnetic transition temperature at 225 K, there is an increase of the intensity of the low energy phonons around

20 meV associated with the dynamics of the Fe atoms. The low energy vibrations exhibit a significant Q dependence up to about 848 K, indicating a persistence of the paramagnetic spin fluctuations up to very high temperatures. GaFeO₃ is not subject to any structural high temperature phase transition. However, the increase of the distortion amplitudes of the various polyhedral units might be at the origin of the gradual broadening of the stretching modes around 60 meV. The *ab initio* phonon calculations highlighted unambiguously a spin-phonon coupling in GaFeO₃. The enthalpy calculations in various phases showed that the quenching of the Fe magnetic moment leads to the observed high-pressure structural phase transition at 47 GPa. The calculated thermal expansion is in good agreement with the available experimental data.

-
- [1] S. Picozzi and C. Ederer, *J. Phys.: Condens. Matter* **21**, 303201 (2009).
- [2] G. Catalan and J. F. Scott, *Adv. Mater.* **21**, 2463 (2009).
- [3] Ce-Wen Nan, M. I. Bichurin, Shuxiang Dong, D. Viehland, and G. Srinivasan, *J. Appl. Phys.* **103**, 031101 (2008).
- [4] V. V. Pavlov, A. R. Akbashev, A. M. Kalashnikova, V. A. Rusakov, A. R. Kaul, M. Bayer, and R. V. Pisarev, *J. Appl. Phys.* **111**, 056105 (2012)
- [5] W. Eerenstein, N. D. Mathur, and J. F. Scott, *Nature* **442**, 759 (2006)
- [6] J. H. Lee, L. Fang, E. Vlahos, X. Ke, Y. W. Jung, L. F. Kourkoutis, J.-W. Kim, P. J. Ryan, T. Heeg, M. Roeckerath, V. Goian, M. Bernhagen, R. Uecker, P. C. Hammel, K. M. Rabe, S. Kamba, J. Schubert, J. W. Freeland, D. A. Muller, C. J. Fennie, P. Schiffer, V. Gopalan, E. J. Halperin, and D. G. Schlom, *Nature* **466**, 954 (2010).
- [7] T. Kimura, T. Goto, H. Shintani, K. Ishizaka, T. Arima, and Y. Tokura *Nature* **426**, 55 (2003).
- [8] B. B. V. Aken, T. T. M. Palstra, A. Filippetti, and N. A. Spaldin, *Nature Materials* **3**, 164 (2004).
- [9] R. Ramesh and N. A. Spaldin, *Nat. Mater.* **6**, 21 (2007).
- [10] N. Hur, S. Park, P. A. Sharma, J. S. Ahn, S. Guha, and S-W. Cheong, *Nature* **429**, 392 (2004).
- [11] N. Ikeda, H. Ohsumi, K. Ohwada, K. Ishii, T. Inami, K. Kakurai, Y. Murakami, K. Yoshii, S. Mori, Y. Horibe, and H. Kito, *Nature* **436**, 1136 (2005).
- [12] D. V. Efremov, J. V. D. Brink, and D. I. Khomskii, *Nature Materials* **3**, 853 (2004).
- [13] M. Zbiri, H. Schober, N. Choudhury, R. Mittal, S. Chaplot, S. Patwe, S. Achary, and A. Tyagi, *Appl. Phys. Lett.* **100**, 142901 (2012).
- [14] T. Kimura, S. Kawamoto, I. Yamada, M. Azuma, M. Takano, and Y. Tokura, *Phys. Rev. B* **67**, 180401(R) (2003).
- [15] T. Arima, D. Higashiyama, Y. Kaneko, J. P. He, T. Goto, S. Miyasaka, T. Kimura, K. Oikawa, T. Kamiyama, R. Kumai, and Y. Tokura, *Phys. Rev. B* **70**, 064426 (2004).
- [16] K. Kelm and W. Mader, *Z. Anorg. Allg. Chem.* **631**, 2383 (2005).
- [17] R. B. Frankel, N. A. Blum, S. Foner, A. J. Freeman, and M. Schieber, *Phys. Rev. Lett.* **15**, 958 (1965).
- [18] M. J. Han, T. Ozaki, and J. Yu, *Phys. Rev. B* **75**, 060404 (2007); D. Stoeffler, *J. Phys.: Condens. Matter* **24**, 185502 (2012).
- [19] J. P. Remeika, *J. Appl. Phys. Suppl.* **31**, 263S (1960).
- [20] S. Mukherjee, A. Roy, S. Auluck, R. Prasad, R. Gupta, and A. Garg, *Phys. Rev. Lett.* **111**, 087601 (2013); A. Thomasson, S. Cherifi, C. Lefevre, F. Roulland, B. Gautier, D. Albertini, C. Meny, and N. Viart, *J. Appl. Phys.* **113**, 214101 (2013).
- [21] R. Saha, A. Shireen, Sharmila N. Shirodkar, M. S. Singh, U. V. Waghmare, A. Sundaresan, and C. N. R. Rao, *Inorg. Chem.* **50**, 9527 (2011).
- [22] P. Kumar, A. Bera, D. V. S. Muthu, S. N. Shirodkar, R. Saha, A. Shireen, A. Sundaresan, U. V. Waghmare, A. K. Sood, and C. N. R. Rao, *Phys. Rev. B* **85**, 134449 (2012).
- [23] U. Staub, Y. Bodenthin, C. Piamonteze, S. P. Collins, S. Koohpayeh, D. Fort, and S. W. Lovesey, *Phys. Rev. B* **82**, 104411 (2010).
- [24] Z. H. Sun, B. L. Cheng, S. Dai, L. Z. Cao, Y. L. Zhou, K. J. Jin, Z. H. Chen, and G. Z. Yang, *J. Phys. D: Appl. Phys.* **39** 2481 (2006).
- [25] K. Sharma, V. Raghavendra Reddy, A. Gupta, S. D. Kaushik, and V. Siruguri, *J. Phys.: Condens. Matter* **22**, 146005 (2010).
- [26] S. Mukherjee, A. Garg, and R. Gupta, *J. Phys.: Condens. Matter* **23**, 445403 (2011).
- [27] K. Sharma, V. Raghavendra Reddy, A. Gupta, S. D. Kaushik, and V. Siruguri *J. Phys.: Condens. Matter* **24**, 376001 (2012).
- [28] S. K. Mishra, R. Mittal, Ripandeep Singh, S. L. Chaplot, M. Zbiri, T. Hansenk, and H. Schober, *J. Appl. Phys.* **113**, 174102 (2013).
- [29] R. Arielly, W. M. Xu, E. Greenberg, G. Kh. Rozenberg, M. P. Pasternak, G. Garbarino, S. Clark, and R. Jeanloz, *Phys. Rev. B* **84**, 094109 (2011).
- [30] S. E. Hahn, A. A. Podlesnyak, G. Ehlers, G. E. Granroth, R. S. Fishman, A. I. Kolesnikov, E. Pomjakushina, and K. Conder, *Phys. Rev. B* **89**, 014420 (2014).
- [31] S. M. Shapiro, J. D. Axe, and J. P. Remeika, *Phys. Rev. B* **10**, 2014 (1974).
- [32] S. Artyukhin, M. Mostovoy, N. P. Jensen, D. Le, K. Prokes, V. G. de Paula, H. N. Bordallo, A. Maljuk, S. Landsgesell, H. Ryll, B. Klemke, S. Paeckel, K. Kiefer, K. Lefmann, L. T. Kuhn, and D. N. Argyriou, *Nat. Mater.* **11**, 694 (2012).

- [33] M. Zbiri, R. Mittal, S. Rols, Y. Su, Y. Xiao, H. Schober, S. Chaplot, M. Johnson, T. Chatterji, Y. Inoue, S. Matsuishi, H. Hosono, and T. Brueckel, *J. Phys.: Condens. Matter* **22**, 315701 (2010).
- [34] R. Mittal, M. K. Gupta, S. L. Chaplot, M. Zbiri, S. Rols, H. Schober, Y. Su, Th. Brueckel, and T. Wolf, *Phys. Rev. B* **87**, 184502 (2013).
- [35] D. L. Price and K. Skold, in *Neutron Scattering*, edited by K. Skold and D. L. Price (Academic Press, Orlando, 1986), Vol. 35; A. J. M. Carpenter and D. L. Price, *Phys. Rev. Lett.* **54**, 441 (1985); S. Rols, H. Jobic, and H. Schober, *Compt. Rend. Phys.* **8**, 777 (2007).
- [36] <http://www.ncnr.nist.gov>; V. F. Sears, *Neutron News* **3**, 29 (1992); A.-J. Dianoux and G. Lander (eds.), *Neutron Data Booklet*, Institut Laue-Langevin (Grenoble, France, 2002).
- [37] G. Kresse and D. Joubert, *Phys. Rev. B* **59**, 1758 (1999).
- [38] A. Dal Corso, *Phys. Rev. B* **82**, 075116 (2010).
- [39] P. Hohenberg and W. Kohn, *Phys. Rev.* **136**, B864 (1964).
- [40] W. Kohn and L. J. Sham, *Phys. Rev.* **140**, A1133 (1965).
- [41] G. Kresse and J. Furthmüller, *Comput. Mater. Sci.* **6**, 15 (1996).
- [42] J. P. Perdew, K. Burke, and M. Ernzerhof, *Phys. Rev. Lett.* **77**, 3865 (1996).
- [43] J. P. Perdew and A. Zunger, *Phys. Rev. B* **23**, 5048 (1981).
- [44] S. L. Dudarev, G. A. Botton, S. Y. Savrasov, C. J. Humphreys, and A. P. Sutton, *Phys. Rev. B* **57**, 1505 (1998).
- [45] V. I. Anisimov, F. Aryasetiawan, and A. I. Lichtenstein, *J. Phys.:Condens. Matter* **9**, 767 (1997).
- [46] M. J. Han, T. Ozaki, and J. Yu, *Phys. Rev. B* **73**, 045110 (2006).
- [47] M. P. J. Punkkinen, K. Kokko, W. Hergert, and I. J. Vayrynen, *J. Phys.: Condens. Matter* **11**, 2341 (1999).
- [48] G. Rollmann, A. Rohrbach, P. Entel, and J. Hafner, *Phys. Rev. B* **69**, 165107 (2004).
- [49] A. Bandyopadhyay, J. Velez, W. H. Butler, S. K. Sarker, and O. Bengone, *Phys. Rev. B* **69**, 174429 (2004).
- [50] K. Parlinski, Phonon Software (2003).
- [51] M. Marezio, J. P. Remeika, and P. D. Dernier, *Acta Cryst. B* **26**, 2008 (1970).
- [52] H. Boysen and F. Altorfer, *Acta Cryst. B* **50**, 405 (1994).
- [53] R. Mittal, S. L. Chaplot, and N. Choudhury, *Progress of Materials Science* **51**, 211 (2006).
- [54] G. Venkatraman, L. Feldkamp, and V. C. Sahni, *Dynamics of Perfect Crystals* (MIT, Cambridge, 1975).